J Am Oil Chem Soc (2009) 86:1–17
DOI 10.1007/s11746-008-1317-8

REVIEW

EPR Investigations of Spin-Probe Dynamics in Aqueous Dispersions of a Nonionic Amphiphilic Compound

Kouichi Nakagawa

Received: 15 July 2008 / Revised: 6 October 2008 / Accepted: 27 October 2008 / Published online: 27 November 2008

Abstract Dynamics of various spin probes in aqueous dispersions of nonionic amphiphilic compound, [poly(oxyethylene) hydrogenated castor oil, HCO], were investigated by EPR (electron paramagnetic resonance) and saturation recovery (SR) spectroscopies. Partitioning, rotational correlation time (τ_R), rotational diffusion coefficient, and electron spin-lattice relaxation time (T_{1e}) in dispersions of the HCO membrane were obtained. The partitioning of water soluble spin probes, DTBN and TEMPO, in the aqueous and vesicle phases was determined by an EPR linewidth simulation as a function of temperature. The results suggest that DTBN and TEMPO have a similar partitioning in the vesicle phase throughout the temperatures studied. The longer τ_R and shorter T_{1e} ($\sim$0.33 μs) values of DTBN in the vesicle phase were obtained, and could be attributed to the probe environment in the membrane. The simulation results for fast tumbling probes were quite different from those of conventional intensity analysis (spectral parameter, *f*). Thus, the simulation and T_{1e} analyses have provided a quantitative understanding of the probe dynamics in both phases. Aliphatic spin probes, doxylstearic acids (DSAs) and 3β-doxyl-5α-cholestane (CHL), were used for monitor of various membrane motions. The EPR spectra were quantitatively analyzed by a slow tumbling simulation. The rotational diffusion coefficients and order parameter were obtained by the simulation. In addition, the direct observations of the behavior of the probes were measured by SR method. The results were consistent with T_{1e} obtained for spin probes. Thus, the quantitative results regarding EPR, SR method, various simulation analyses have provided detailed information regarding physicochemical properties of the various moieties of the probe region in the amphiphilic compound.

Keywords EPR · Saturation recovery · Spin probe · Rotational diffusion coefficients · Spin-lattice relaxation time · Activation energy · Vesicle · Aqueous phase · Partitioning · Dispersion · Correlation time · Order parameter · Simulation · Dynamics · Amphiphilic compound · Membrane

Introduction

Electron paramagnetic resonance (EPR) or electron spin resonance (ESR) has the same basic scientific background as NMR. The EPR spin probe methodology is advantageous for studying molecular dynamics in biological membranes on time scales from nanoseconds to milliseconds [1]. Dynamics of spin probes incorporated in the membranes provide very important clues for understanding the physicochemical characteristics. Knowledge of regional motions is crucial to the quantitative understanding the individual membrane properties. In addition to the membranes, polymeric materials have been examined for spin probe dynamics in polymer aggregates [2, 3], rotational diffusion, and conformation of polyelectrolytes [4, 5].

Reliable information of the biological membrane can also be obtained by fluorescence spectroscopy [6]. Investigations of the head group region have been performed using fluorescence in conjunction with probes. The fluorescence probes having a large aromatic ring and very different chemical structure relative to the lipid components are normally used. Furthermore, the sensitivity of the

K. Nakagawa (✉)
RI Research Center, Fukushima Medical University,
1 Hikarigaoka, Fukushima 960-1295, Japan
e-mail: nakagawa@fmu.ac.jp

fluorescence techniques is low in the order of the micromolar concentration of the probe. On the other hand, 9-GHz EPR is not only very sensitive to concentration in the order of micro to nano-molar concentrations but also the chemical structures of the aliphatic spin probes are more similar to the lipids. Thus, EPR has excellent techniques for investigating new insights into motional behavior of the various membranes. A modern simulation analysis in conjunction with the spin probe method can extract quantitative information regarding various probe motions in the membranes [7].

The macroscopic and local viscosity of the environment profoundly influences the rate of lipid molecular reorientation. The behavior of the lipid molecule in the membrane is strongly influenced by the temperature. Changes in the viscosity are reflected in the EPR linewidth as well as the lineshape because of anisotropy in the g value and in the ^{14}N hyperfine structure. The conventional order parameter calculated using the hyperfine coupling values gives limited information regarding the chain ordering of the membranes [8, 9]. Subtle changes in the EPR line shape do not always reflect the hyperfine coupling values. The lineshape of the EPR signal, which contains all information regarding the probe environments, can be quantitatively analyzed by a computational method to determine the probe dynamics, such as chain ordering as well as fluidity [10]. A computational analysis of the EPR spectra gives new insights concerning membrane behavior. In addition, an EPR investigation of the thermal behavior of the membrane chain provides details regarding the membrane characteristics.

For over 25 years, the various properties of aliphatic spin probes (doxylstearic acid spin probes) incorporated in the membrane have been discussed as the results of conventional analyses [8, 9, 11]. The conventional method determined the chain ordering of biological membranes employing EPR hyperfine coupling constants of lipid incorporated probes [9, 11]. The conventional analyses of the membrane organization, such as spectral parameter and order parameter, provide qualitative information about the membrane. Therefore, the detailed membrane characteristics should be extensively investigated by means of careful analyses of the corresponding EPR observations.

Water soluble spin probes such as TEMPO, partitioned between the aqueous and the fluid hydrophobic phase of biological membranes dispersed in water, were utilized to construct the phase diagram and study phase separation [8, 9]. Overlapped and linewidth altering EPR signals of the aqueous and vesicle phases were analyzed using a linewidth-calculated program to determine the partitioning quantitatively. The various phospholipids were investigated to obtain membrane properties such as phase transition and fluidity using the overlapped spectra. The phase diagrams of aqueous dispersions for the binary mixture were studied using the spectral parameter of TEMPO and led to a detailed discussion of membrane characterization.

Detailed motions including chain ordering of aliphatic spin probes in the membrane were investigated [12, 13]. Different positions and motions of the probe moiety show different temperature sensitivity based on the activation energy obtained. For perpendicular behavior, the area near the end of the membrane is sensitive to temperature. In contrast, in the area near the head group, parallel motion is sensitive to temperature [12]. The activation energy calculated using the τ_R values can be associated with the segmental micro-viscosity around the spin probe in the membrane, and the molecular dynamics of the spin probes studied in relation to T_{1e}. Furthermore, physicochemical characterization of the vesicle for the nonionic amphiphilic compound HCO could lead to detailed understanding of the bilayer behavior as well as its characteristics. Temperature dependence in relation to dynamic structure of membranes is an important subject in colloid interface and membrane sciences. Recently, it has been found that quantitative EPR investigations (e.g. an EPR spectral simulation) will lead to detailed understanding of the bilayer behavior directly related to characteristics of the macromolecules [3, 4, 12, 14].

The direct measurement of spin probe moieties in a membrane can be performed using a SR (saturation recovery) apparatus. SR is the technique for electron spin-lattice relaxation measurements in EPR. Various motional processes contribute to electron spin-lattice relaxation such as tumbling motion and intramolecular motions. The spin-lattice relaxation times (T_{1e}) of aliphatic spin probes became shorter when the position of the probe moved toward the inner membrane [12, 13]. The shorter T_{1e} implies more motional interaction between the probe and the membrane chain. In addition, the T_{1e} values of the probes supported perpendicular diffusion coefficients obtained by spectral simulation [14]. The spin dynamics were also consistent with the observed EPR lineshape.

Nonionic amphiphiles are widely recognized as synthetic tailor-made lipids in view of their safety and ease of molecular structural design. Especially, nonionic surface active agents have been of great interest in the fields of cosmetics as well as pharmaceuticals. In drug encapsulation, vesicle formation of the agent is necessary. Nontoxic and naturally degradable substances are also desired. Recently, poly(oxyethylene) hydrogenated castor oil (termed HCO), which is derived from one of the lipids and related natural products, was found to form vesicles [15]. A stable multi-lamellar vesicle with an average diameter of $\sim$500 nm was observed. HCO is a physiologically nontoxic and naturally degradable substance. Furthermore,

HCO has a unique chemical structure among triglyceride derivatives. It consists of a uniform fatty-portion structure embodying oxyethylene groups unlike most naturally occurring triglycerides, which are composed of mixed fatty-portions. Hence, HCO is a very interesting compound for investigation of chain motions [12, 13, 16].

In this review, EPR studies of a modern simulation for EPR results in addition to a newly developed SR were applied to reveal detailed probe behavior in the head group region of HCO membranes. The slow-motional spectral simulation was used to extract information regarding the detailed chain ordering. The simulation provides an order parameter (S_0) along with two rotational dynamic parameters, parallel and perpendicular rotational diffusion coefficients [12, 13]. The quantitative S_0 values together with the two dynamic parameters at the different positions of the membrane are discussed in comparison with the conventional hyperfine analysis. In addition, the direct motional information between a probe and the membrane was obtained using an advanced SR technique. Detailed rotational diffusion coefficients and spin-lattice relaxation times of spin probes in aqueous dispersions of the HCO membrane were analyzed as a function of temperature. The spin-lattice relaxation times directly reflect the motional interaction between the probe and the membrane chains. Advanced EPR techniques are advantageous for the investigation of regional behavior of the membrane. Linewidth as well as lineshape were carefully considered to determine the rotational diffusion. The detailed probe environment in the membrane is discussed in relation to activation energies as well as the spin-lattice relaxation time.

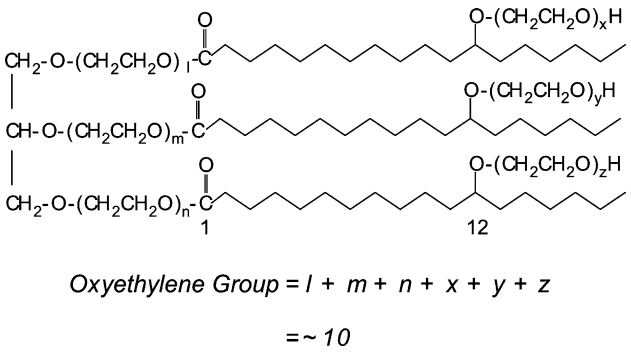

Fig. 1 Chemical structures of poly(oxyethylene) (10) HCO is depicted. It is notable that the fatty portion of HCO is composed of 18 carbon atoms. Half of the oxyethylene groups are attached to the 12th carbon from the carbonyl carbon of the main chain

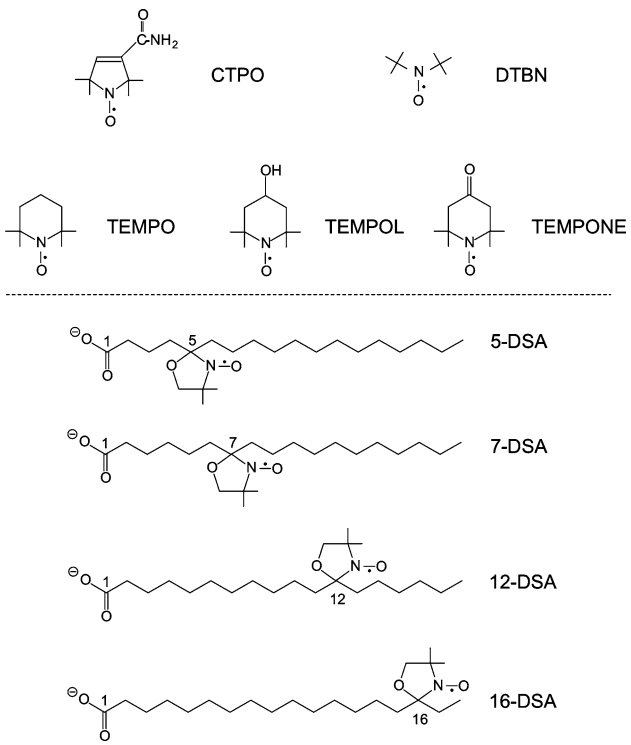

Fig. 2 Chemical structures of various spin probes

Materials and Methods

Materials

Poly(oxyethylene) hydrogenated castor oil (HCO) of the highest quality was donated by Nikko Chemicals Co. Ltd (Tokyo, Japan) and used as received. The HCO had about 10 mol of oxyethylene moieties per mole of the compound. The molecular structures of HCO and the spin probes used in this study are depicted in Figs. 1 and 2. The oxyethylene groups are attached to the 12th carbon from the carbonyl carbon of the main chain.

Basically two kinds of spin probes (spin labels) were used in the investigation. The first kind consists of spin probes with low molecular weights, so-called small spin probes. The other one consists of spin probes with high molecular weights, so-called large spin probes (or aliphatic spin probes). The following small spin probes were utilized: di-*tert*-butyl nitroxide (DTBN), 2,2,6,6-tetramethylpiperidine-1-oxyl (TEMPO), 4-hydroxy-2,2,6,6-tetramethylpiperidine-1-oxyl (TEMPOL), 4-oxo-2,2,6,6-tetramethylpiperidine-1-oxyl (TEMPONE), and 3-(aminomethyl)-proxyl (CTPO) (proxyl: 2,2,5,5-tetramethyl-1-pyrolidinyloxyl), were obtained from Sigma–Aldrich Co. and used as received.

The following large spin probes were utilized: 5-(4,4-dimethyl-3-oxazolidinyl)oxy-octadecanoic acid, so-called 5-doxylstearic acid (5-DSA), 7-doxylstearic acid (7-DSA), 12-doxylstearic acid (12-DSA), 16-doxylstearic acid (16-DSA), and 3β-doxyl-5α-cholestane (CHL) were also obtained from Sigma–Aldrich Co. The chemical structures

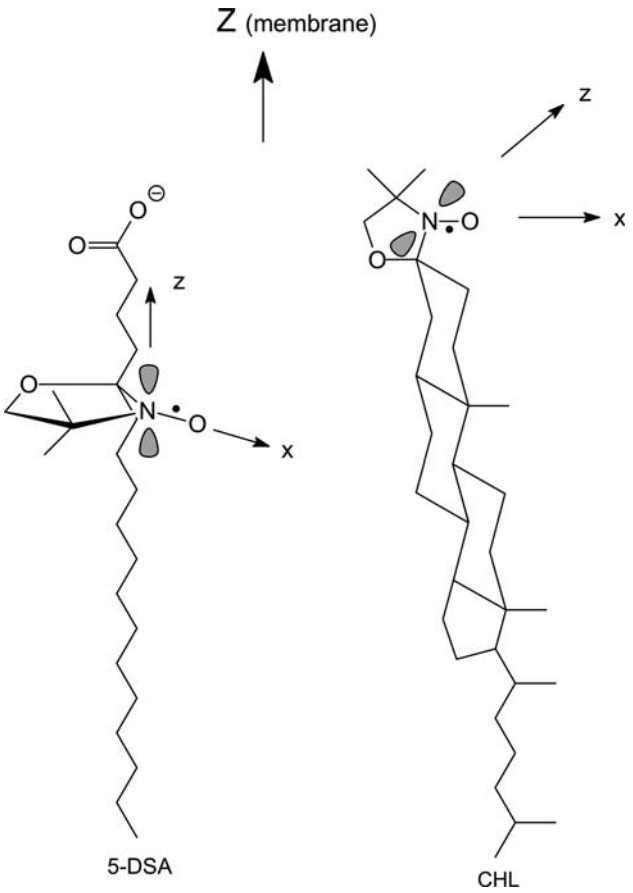

Fig. 3 Exact coordination of the spin probes, 5-DSA and CHL, for the NLLS calculations are presented. The *z*-axis is the membrane director

of the spin probes used in this investigation are depicted in Figs. 2 and 3. Lecithin (phosphatidylcholine, PC) from egg was purchased from Wako Pure Chemical Ind. Ltd, Japan. All chemicals were of the highest grade obtainable and used as received.

Sample Preparations

Two sample preparations were used at ambient temperature. Method one: a weighed amount of HCO was dissolved in a few milliliters of chloroform [17]. The weighed spin probe was dissolved in ~0.3 mL of chloroform and mixed with the HCO chloroform solution. After evaporation of the chloroform in a rotary evaporator, a 10 wt% dispersion of the HCO/spin probe in distilled water (HPLC grade, Nacalai tesque, Japan) was prepared. An aliquot of the dispersion solution was used for the EPR measurements. The final concentration of the spin probe was approximately 10 μM for the CW (continuous wave) EPR and 100 μM for the saturation recovery (SR) measurements. It should be noted that slightly different doping concentrations of the small spin probes did not change the HCO properties.

Method two: HCO was dispersed in water to ~10 wt%, and a spin probe was added to the solution. A test tube containing the dispersion solution was agitated on a vortex mixer until completely dispersed. The final concentration of the spin probe was the same as that in method one. For CW EPR measurements, the dispersion solution was placed in a glass capillary (i.d. 0.9 mm) and one end was sealed.

The spin probes were also incorporated in the PC from egg in the same manner as the HCO. A ~0.8 wt% dispersion of PC/probe in 1 mM Tris–HCl buffer solution under a nitrogen atmosphere was prepared. The test tube containing the dispersion solution was agitated on a vortex mixer until completely dispersed. An aliquot of the dispersion was used for EPR measurements. The final concentration of the spin probe was approximately 100 μM for the measurements [18].

Deoxygenation

For CW EPR, the sample solutions (~0.15 mL) were deoxygenated for about 15 min in an AtmosBag (Aldrich) and the solutions were put into capillaries (i.d., 0.9 mm; o.d., 1.4 mm; Nippon Rikagaku Kikai Co. Ltd, Japan). A sample capillary was inserted in a 3-mm EPR tube (JEOL Datum Co. Ltd, Japan) in the AtmosBag and taped around the tube cap.

Degassing of SR measurements was carried out using Teflon tubes to achieve degassing in the following manner. Two Teflon tubes were inserted side-by-side in a 4-mm EPR tube. One Teflon tube (i.d., 0.96 mm; o.d., 1.56 mm) contained the sample solution. Nitrogen was passed through the second Teflon tube (i.d., 1.5 mm; o.d., 2 mm) to purge oxygen from the solution [12, 13].

CW EPR Measurements

Electron paramagnetic resonance measurements were made with a 9-GHz JEOL FE 1XG spectrometer with a TE_{011} cylindrical cavity. The sample temperature was controlled by a nitrogen gas flow through the Dewar vessel using a JEOL ES-DVT system. The EPR signals were digitized using a Scientific Software Services data-acquisition system (Michigan, USA). The microwave frequency was measured using an EMC-14 X-band microwave frequency counter (Echo Electronics Co., Ltd, Japan). Typical conditions were as follows: microwave frequency, 9.185 GHz; microwave power, 10 mW; modulation amplitude, 0.08 mT; time constant, 0.1 s; sweep rate, 0.312 mT per minute.

Rotational Correlation Time for the Fast-Tumbling Spin Probe

Various practical methods have been developed for obtaining the correlation time for local molecular motion based on changes in the amplitude, position, and widths of EPR lines. Rotational correlation times (τ_R) on the order of 10^{-10} s can be estimated from the spectra of a nitroxide spin probe using the following equation [19],

$$\tau_R = \left(\frac{2\sqrt{3}g_{iso}\beta_e}{\hbar b^2}\right)\left(\sqrt{\frac{I_0}{I_{+1}}} + \sqrt{\frac{I_0}{I_{-1}}} - 2\right)\Delta H_{pp0}, \quad (1)$$

where β_e is the electron Bohr magneton, $\hbar$ is Plank's constant, I is the peak amplitude, and the subscripts $+1$, 0, -1 are nuclear quantum numbers for ^{14}N. ΔH_{pp0} is the peak-to-peak line-width of the centerline. The values of g_{iso} and b are calculated from the parameters for the immobilized spin probe:

$$g_{iso} = \frac{1}{3}\left(g_{xx} + g_{yy} + g_{zz}\right), \quad (2)$$

$$b = \frac{2}{3}\left[A_{zz} - \frac{1}{2}\left(A_{xx} + A_{yy}\right)\right]. \quad (3)$$

Calculations of τ_R for the spin probes were made using the magnetic principal values [20]. The parameters I_{+1}, I_0, I_{-1}, and ΔH_{pp0} obtained from the experimental spectra were used to calculate τ_R. It is noted that Eq. 1 is used for the relatively fast motion of small spin probes, but not for the slower motion of various aliphatic spin probes.

Spectral Simulation of the Fast-Tumbling Spin Probe

The overlapped EPR signal from different environments was simulated as the sum of two components: the aqueous and vesicle phases. The linewidth of the signal can vary under certain probe environments. When a line broadening arises from incomplete averaging of the g factor and the hyperfine coupling interactions in the limit of rapid tumbling in solution, the linewidth varies with the magnetic quantum number (M) of one component. The dependence of the linewidth on M_I of an individual hyperfine line is given in the motional narrowing region by the following expression [21]:

$$\Gamma = A + BM_I + CM_I^2, \quad (4)$$

where Γ is the linewidth, M_I is the nuclear spin quantum number, and A, B, and C are the functions of nitrogen g-factor and hyperfine tensor. The A term contributes to the overall spectrum, the B term causes anisotropy in the spectrum, and the C term broadens the spectrum symmetrically. The square dependence on M_I arises from the electron-nuclear spin dipole interaction and the linear dependence on M_I is due to the cross product of the anisotropic dipolar and g tensor interactions modulated by the rotational motion. The last term is responsible for the low intensity of the high-field line. As a result, the high-field linewidths are much more sensitive to changes in the nitroxide tumbling motion.

EPR spectra were simulated using the computer program, ASYM [21]. The simulation program is composed of two parts: the aqueous and vesicle triplets. Each phase has three terms and nitrogen hyperfine value. The nitrogen hyperfine splitting was treated as second order. Unresolved proton hyperfine splitting was modeled by varying the Lorentzian and Gaussian contributions to the lineshape. The dependence on the nitrogen linewidth M_I is described by the Eq. 4. Linewidth parameters (A, B, and C) were adjusted to obtain best-fit simulated spectra. The best-fit spectra obtained by varying the weightings of the spectra in the two phases were chosen on the basis of minimization of the residual between the experimental and the simulated spectra. Based on the simulated spectra of the two phases, aqueous and vesicle, partitioning of the spin probes at each temperature was determined.

Spectral Simulation of the Slow Tumbling Spin Probe

The slow-tumbling motions of the aliphatic spin probes were calculated using the nonlinear least-squares fitting program called NLLS to analyze the EPR spectra based on the stochastic Liouville equation [14, 22]. The simulation of the EPR spectra for spin probes incorporated into multilamellar vesicles was carried out using a microscopically ordered but macroscopically disordered (MOMD) model [23, 24]. This model is based on the characteristics of the dynamic structure of lipid dispersions. For example, lipid molecules are preferentially oriented by the local structure of the bilayer, but the lipid bilayer fragments are overall distributed randomly. The spectrum from the sample can be regarded as a superposition of the spectra from all of the fragments.

The lipid and the probe molecules in the membrane bilayer experience ordering potentials, which restrict the amplitude of the rotational motion. The orienting potential in a lipid bilayer, $U(\Omega)$, determines the orientational distribution of molecules with respect to the local ordering axis of the membrane bilayer. It can be expressed as an expansion in generalized spherical harmonics [25],

$$-U/kT = c_0^2 D_{00}^2(\Omega) + c_2^2\left(D_{02}^2(\Omega) + D_{0-2}^2(\Omega)\right) + \cdots, \quad (5)$$

where $\Omega = (\alpha, \beta, \gamma)$ are the Euler angles between the molecular frame of the rotational diffusion tensor and the local director frame. The c_0^2 and c_2^2 are dimensionless potential energy coefficients, k is the Boltzmann constant, and T is the absolute temperature.

There are two axes systems in the calculation of the rotational dynamics and orientational ordering of the spin probe. In the magnetic frame, the z-axis is parallel to the $2P_z$ orbital of the N atom for doxylstearic acid, which is perpendicular to the N–O bond of the nitroxide probe as shown in Fig. 3. Then, the y-axis in the magnetic frame is perpendicular to both x- and z-axes, forming a right-handed axis frame. In the molecular frame, the z-axis is parallel to the symmetry axis of the probe molecule. For 5-DSA, obviously, the z-axis is parallel to the long hydrocarbon chain, which coincides with the z-axis in the magnetic frame.

The rigidity (chain ordering), S_0, is defined as

$$S_0 = \langle D_{00}^2 \rangle = \left\langle \frac{1}{2}(3\cos^2\gamma - 1) \right\rangle = \frac{\int d\Omega \exp(-U/kT) D_{00}^2}{\int d\Omega \exp(-U/kT)}, \quad (6)$$

which measures the angular extent of the rotational diffusion of the nitroxide moiety. Gamma (γ) is the angle between the rotational diffusion symmetry axis and the z-axis of the nitroxide axis system. The local or microscopic ordering of the nitroxide spin probe in the membrane is characterized by the S_0 value. A larger S_0 value indicates more restricted motion. Therefore, S_0 reflects the local ordering of bilayer molecules in the membrane.

Dynamics of the probe are described by the following parameters: rotational diffusion rates ($R_\perp$ and $R_\parallel$) along axes perpendicular and parallel to the molecular symmetry axes [25]. The perpendicular component represents the rotational wagging motion of the long axis of the hydrocarbon chain, whereas for CHL the $R_\perp$ is the wagging motion of the long molecular axis. This component can be correlated with the rotational correlation time [$\tau_R \approx 1/(6R_\perp)$] [14]. In the calculation of experimental spectra, the principal components for the probes obtained by the previous values were used [10, 26].

Saturation Recovery (SR) Measurements

The electron spin-lattice relaxation time (T_{1e}) was measured by a home-built saturation recovery (SR) spectrometer equipped with a 5-loop-4-gap resonator (LGR) [27, 28]. The klystron was locked via an AFC circuit to a high-Q cylindrical external reference cavity. The EPR signal was amplified by a low-noise GaAsFET amplifier and detected by use of a double-balanced mixer. No magnetic field modulation was used. The sample temperature was controlled by a Varian V-6040 and nitrogen gas passed over the LGR. The temperature was monitored with a thermocouple positioned immediately above the resonator. The magnetic field for recording the recovery signal was set on the centerline for the spin probe. Artifacts were removed by subtracting an instrumental background response that was measured with the magnetic field set 10 mT higher than for the signal. Under these conditions, the contribution to the recovery due to spectral diffusion is minimized and the time constant is assigned as T_{1e}. The SR signal was observed as an exponential curve. SR curves can be fit with a single-exponential to obtain T_{1e} as follow:

$$SR = A[1 - \exp(-t/T_{1e})], \quad (7)$$

where t is the time, and A is adjustable constant.

Results and Discussion

CW EPR of Small Spin Probes

The CW EPR spectrum of the spin probe (DTBN) in aqueous dispersions consists of two overlapping signals, as presented in Fig. 4a. The small spin probe exists in two sites: the aqueous and vesicle phases [19]. The contributions from the two nitrogen-triplets are best resolved for the high-field hyperfine line. The EPR lines from the probe in the vesicle phase are broader than those from the aqueous phase. The molecular motions of the spin probe in the vesicle are somewhat restricted. In addition, the nitrogen hyperfine coupling of aqueous phase is larger than that of vesicle phase. The EPR spectrum obtained from HCO/DTBN/H_2O shows relatively sharp EPR lines than those of HCO/TEMPO/H_2O. Figure 4b shows typical EPR spectra of TEMPO in an aqueous dispersion of HCO. The spectral difference between the aqueous and vesicle phases is more noticeable than that for TEMPO (Fig. 4b).

Figure 5 shows the EPR spectra of the HCO/TEMPO/H_2O as a function of the temperature. EPR signals of spin probes between the aqueous and vesicle phases were observed. One can easily see the intensity changes of the high-field signals throughout the temperatures studied. Focusing on the high-field lines, the signal amplitude of the vesicle phase increases as the temperature increases while the aqueous peak decreases as temperature increases. This result suggests that the spin probe TEMPO partitions from the aqueous phase to the vesicle phase as temperature increases. The vesicle intensity becomes dominant above ~40 °C. It is notable that the EPR spectrum obtained at 50 °C shows the nitrogen triplet of the vesicle phase is dominant. Similar EPR observations were obtained for the HCO/DTBN/H_2O system.

Careful analyses have been made to determine relative partitioning in two phases. The EPR spectra of the probe partitioning between the two phases were analyzed using the linewidth simulation program (Eq. 4), which takes into account the linewidth change. The representative best-fit

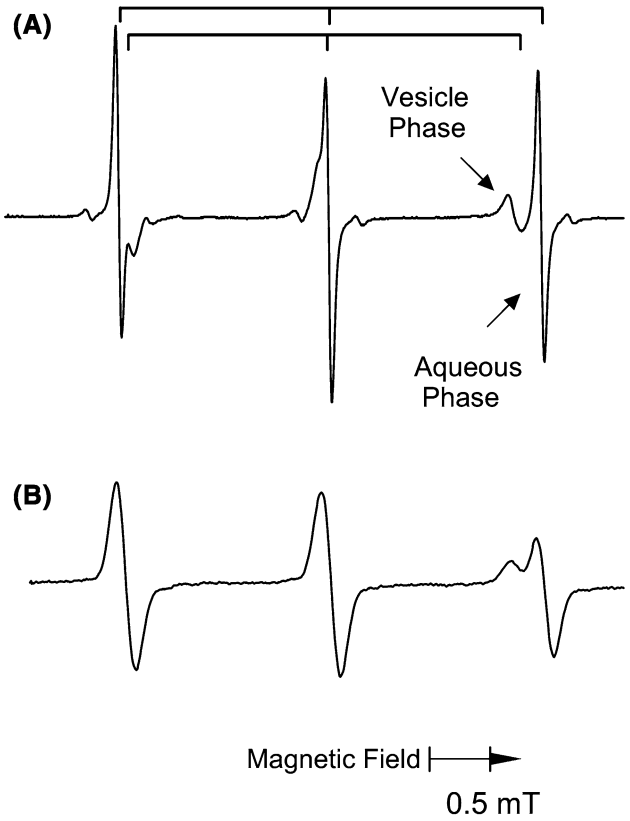

Fig. 4 The EPR spectra of **a** DTBN and **b** TEMPO in aqueous dispersions of HCO. Schematic description regarding the EPR spectra comprising the two triplets: a part of the probe is in the vesicle phase and the remaining is in the aqueous phase. The two sets of hyperfine lines, which are resolved for the high-field hyperfine line, are marked in (**a**)

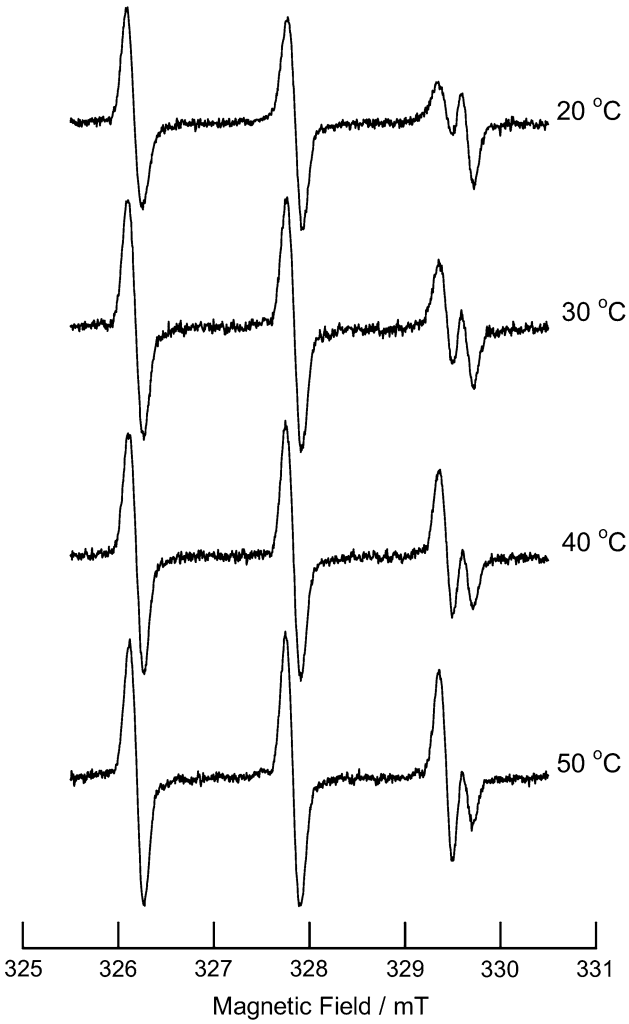

Fig. 5 Temperature dependence of the EPR spectra for the spin probe (TEMPO) in aqueous dispersions of HCO. The temperatures at which the spectra were obtained are indicated

spectra along with the experimental spectra are presented in Fig. 6. The percent of the partitioning was determined by calculating the aqueous and vesicle signals based on the simulation. The obtained partitioning of the spin probes is plotted as a function of the temperature in Fig. 7. The error mainly comes from the sample preparations at ambient temperature as well as a slight difference between the observed and calculated spectra. The simulation results suggest that the partitioning of DTBN and TEMPO in the vesicle phase is similar. The partitioning ($\sim$50%) of the probe at 15 °C increases to 74% at the higher temperature, and shows no abrupt change (Fig. 7). Moreover, the partitioning for both probes shows a similar temperature behavior, and can be in direct relation to the membrane properties. These results are quite different from the previously reported values, which were calculated using the peak intensities [29]. There are two main reasons for the discrepancy. First, the true vesicle intensity is not the same for the overlapped resultant signal. Second, the linewidths of the probe in the vesicle vary when the tumbling motion changes.

Moreover, the EPR spectra of the vesicle phase were obtained by subtracting two spectra under the same experimental temperature and EPR conditions. The reference spectra were used by dissolving spin probes in H_2O. The subtraction was able to eliminate the aqueous peaks. Also, the subtraction was examined with slightly different doping concentrations of the probe. It is noteworthy that slightly different doping concentrations of the probe do not affect the HCO properties. However, it is true that one must have a good reference spectrum for the subtraction method. The representative EPR spectra obtained after subtraction are shown in Fig. 8. Based on the subtracted EPR spectrum, the τ_R was calculated using Eq. 1. The value of τ_R for DTBN changes from 1.2×10^{-10} to 4.9×10^{-10} s at the temperatures studied. The value of τ_R for TEMPO changes from 1.2×10^{-10} to 4.2×10^{-10} s. The longer correlation time ($\sim 4.2 \times 10^{-10}$ s) is an indication of EPR line

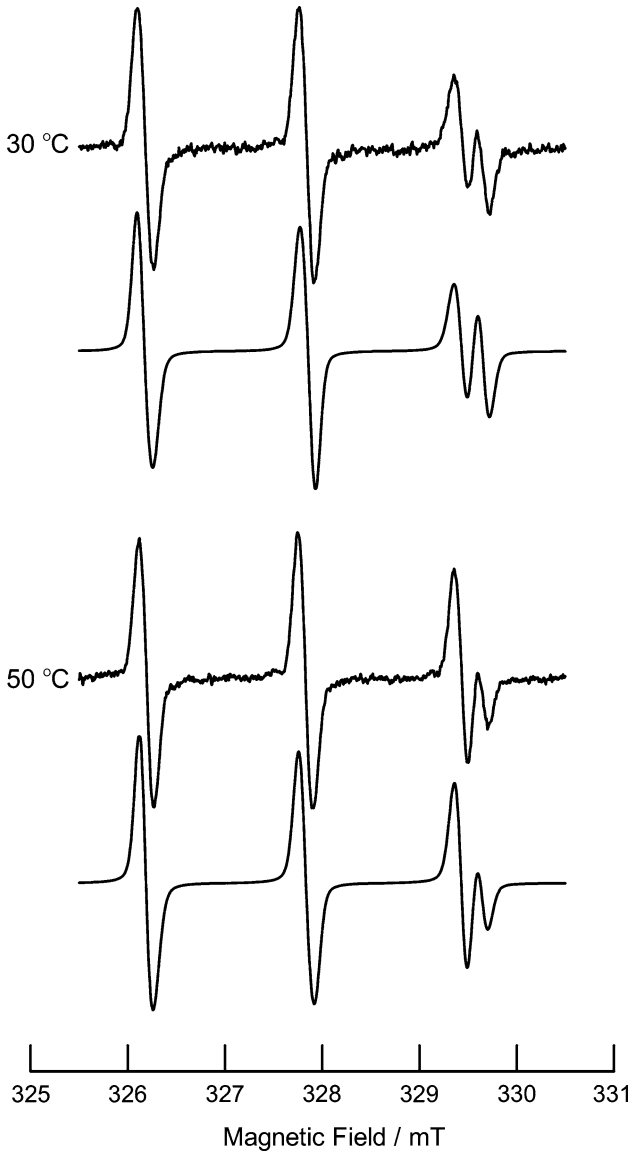

Fig. 6 The representative experimental and simulated EPR spectra for TEMPO in aqueous dispersions of HCO at 30 and 50°C

broadening, especially for the high-field line. This also proves that one should not use peak intensity analysis.

The temperature dependence of the rotational correlation times for DTBN and TEMPO in the vesicle phase is presented as a function of the inverse of the absolute temperature in Fig. 9. It is notable that the correlation time and the partitioning show no drastic change throughout the temperatures studied. An Arrhenius-type equation gives the activation energy for the spin probe in the phase [12, 13],

$$\tau_R = \tau_R^0 \exp\left(\frac{E_a}{RT}\right), \quad (8)$$

where E_a is the activation energy, R is the gas constant, and T is the absolute temperature. The slopes of the plots give

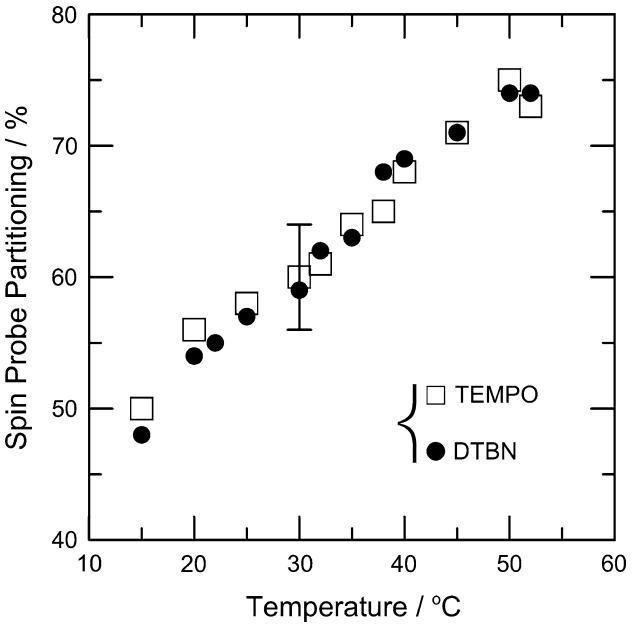

Fig. 7 Partitioning of the vesicle phase for DTBN (*filled circles*) and TEMPO (*open squares*) in H_2O dispersions of HCO as a function of the temperature. The experimental error is indicated

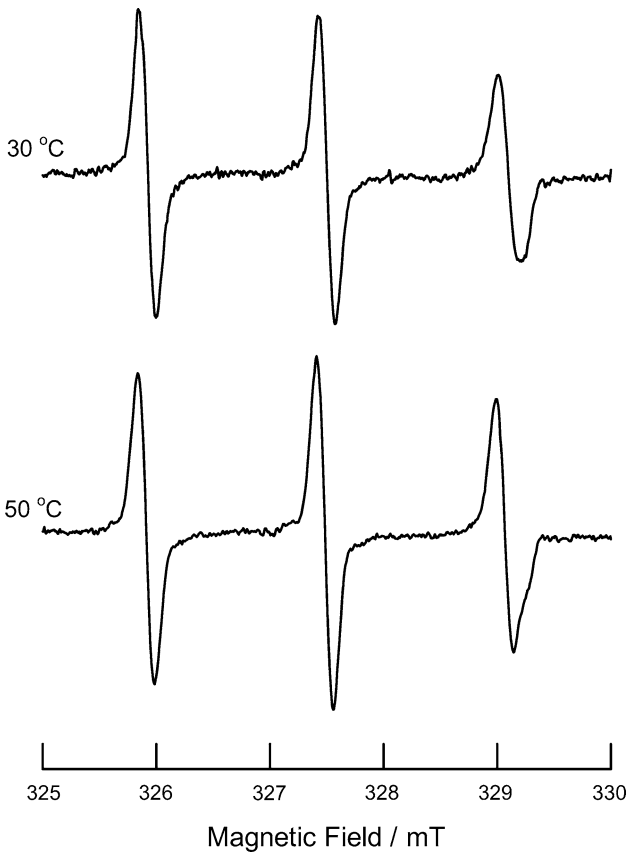

Fig. 8 The representative EPR spectra of the vesicle phase. The EPR spectra were obtained by the subtraction of TEMPO aqueous peaks

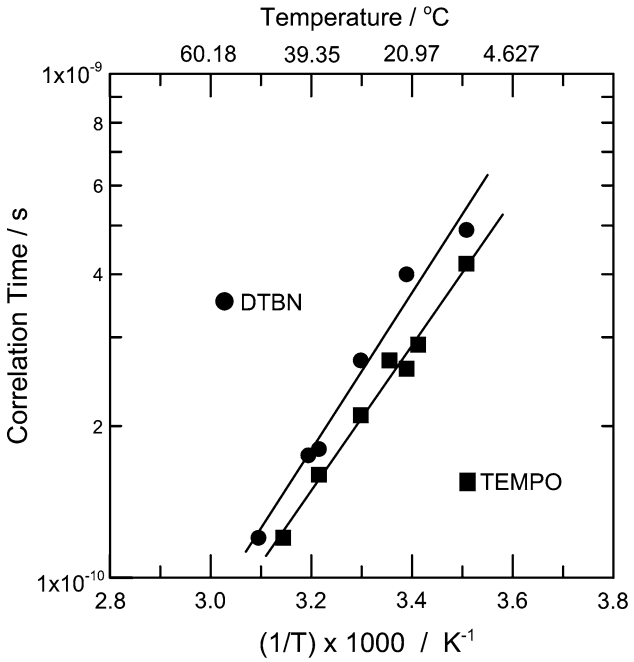

Fig. 9 Temperature dependence of the rotational correlation times for the spin probes, DTBN (*filled circle*) and TEMPO (*filled square*), in the vesicle phase is plotted as a function of the inverse absolute temperature. The activation energies were calculated from the slopes

the activation energies (Fig. 9). The activation energies obtained for TEMPO and DTBN in the membrane are 27.6 ± 1.7 and 29.7 ± 1.7 kJ/mol, respectively. The results suggest that both thermal motions are similar in the membrane. Moreover, the E_a of $\sim$29 kJ/mol] is that in between 24 kJ/mol of 12-DSA and 37 kJ/mol of 16-DSA as listed in Table 1. The activation energy implies that the probe moiety has a similar temperature behavior as well as an approximate location in the membrane.

The calculated τ_R for TEMPONE of the HCO/TEMPONE/H_2O system is approximately 5×10^{-11} s, and is independent of the temperature in the range of 20–50 °C. The value of τ_R is close to the free rotational tumbling time. The estimated τ_R from the spectra for TEMPO and DTBN in the aqueous phase was close to the value. Similar results were obtained for TEMPOL over the same temperature range. The correlation times of TEMPOL and TEMPONE in the dispersions were one order of magnitude faster than that for TEMPO in the vesicle phase.

Table 1 Spin-lattice relaxation time (T_{1e}), rotational diffusion coefficient ($R_\perp$), and order parameter (S_0) of various nitroxide spin probes incorporated in the HCO membrane

Spin probe	T_{1e} (μs)	$R_\perp$ (s^{-1})	E_a (kJ/mol)	S_0	Reference
DTBN (TEMPO)	0.38	–	29	–	[19]
CHL	5.2	7.1×10^7		0.20	[18]
5-DSA	4.6	3.4×10^7	17	0.29	[18]
7-DSA	9.1	1.9×10^7	19	0.68	[12]
12-DSA	5.5	2.6×10^7	24	0.25	[12]
16-DSA	3.6	8.6×10^7	37	0.04	[12]

$R_\perp$ and S_0 values were previously obtained by the EPR simulation. Rotational correlation time (τ_R) $\approx 1/(6R_\perp)$ [14]

Spin-Lattice Relaxation Time (T_{1e}) of Small Spin Probes

In order to further examine the probe motion in the vesicle phase, a direct observation of the interaction between the spin probe and the lattice (membrane) was attempted using SR. The interaction of the probe contributes to the relaxation time in the membrane. T_{1e}'s for the probes in the aqueous and vesicle phases were measured at a magnetic field corresponding to the maximum intensity in the first-integral spectrum for each of the components of the high-field hyperfine line. The typical SR signal from the vesicle peak in the HCO/DTBN/H_2O system at 22 °C is presented in Fig. 10. A single-exponential fit to the experimental data is shown by the dotted line. At this temperature, the signal-to-noise ratio of the SR signal from the vesicle phase is poorer than that for the aqueous phase because of a weaker EPR intensity.

The T_{1e}'s of the probes in the vesicle phase showed very weak temperature dependence in the examined range. The

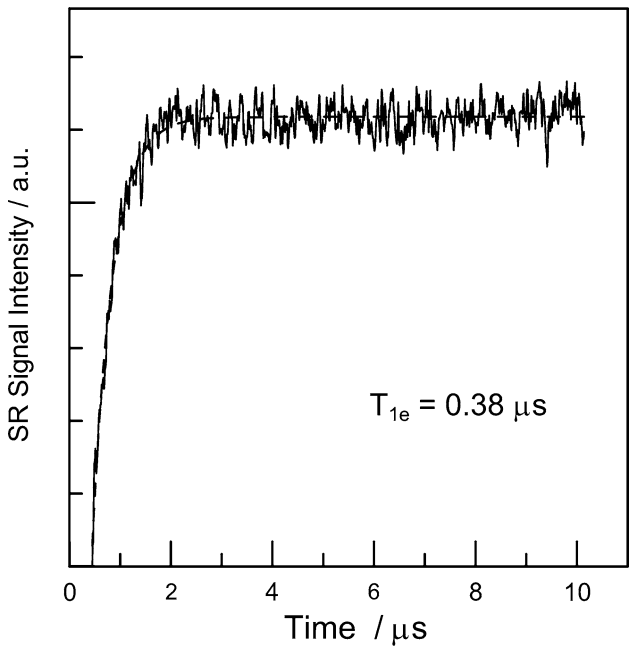

Fig. 10 The typical saturation recovery signal of DTBN in the vesicle phase at 22 °C. The applied magnetic field was set on the magnetic field that corresponds to the maximum intensity in the first-integral spectrum for the vesicle comportment. The *dotted line* indicates a single-exponential fit to obtain T_{1e}

τ_R value of $\sim 10^{-10}$ s (Fig. 9) predicts that T_{1e} is in the vicinity of the minimum value. The minimum value occurs when $\tau_c \omega_0 \approx 1$, where τ_c is the correlation time and ω_0 is the 9-GHz EPR resonance frequency [16]. The temperature dependence of T_{1e} is normally low around this regime. The values of T_{1e} in the vesicle phase are about 0.33 μs in the dispersions. The values of T_{1e} in the aqueous phase are around 0.52 μs. The relaxation time for DTBN in the aqueous phase is consistent with a shorter τ_R in the phase. The T_{1e} values for TEMPO in the aqueous and vesicle phases are about 0.47 μs [30]. There is no clear T_{1e} difference between the two phases, because the overlap of two signals is more significant than that for DTBN (Fig. 4).

The T_{1e} of DTBN in the vesicle phase is shorter than that for the aqueous phase, even considering the experimental error. The shorter T_{1e} ($\sim$0.33 μs) in the vesicle phase can be due to an interaction between the probe and the host lattice. No drastic change in T_{1e} as a function of the temperature was observed. This implies a continuous change of the probe moiety with increasing temperature. The results are attributable to the thermal property of the membrane. In addition, the shorter T_{1e} for DTBN in the vesicle phase could be interpreted as resulting from the location of the probe in the hydrophobic portion of the membrane. This would be consistent with the location of DTBN in the hydrophobic portion of the lipids, as determined by NMR [31]. Thus, a relatively longer τ_R and a shorter T_{1e} for DTBN in the vesicle phase are attributed to the membrane environment. The comparative inhibition of the tumbling motion might account for the results obtained. It is noteworthy that the relaxation also depends not only on the tumbling mobility of the probe, but also on the local concentration. The difficulty is both the local mobility and the concentration change as a function of the temperature.

In order to verify the hydration and/or dehydration effect, T_{1e} of spin probes in a D_2O dispersion solution was measured. Figure 11 also shows a plot of T_{1e} for DTBN in D_2O dispersions. The T_{1e} values of DTBN for the two phases are similar to the case of H_2O. The present SR measurements on T_{1e} of the probes did not show any clear evidence of it based on the results regarding the dispersions of HCO in H_2O and D_2O. Moreover, the recent investigation of aliphatic spin probes in H_2O and D_2O dispersions show no clear difference [12]. Thus, the result suggests that the relaxation process with interaction of H_2O or D_2O is not the major contribution.

The T_{1e} values of TEMPO in the aqueous and vesicle phases are 0.42–0.51 μs throughout the temperatures studied. The values of T_{1e} for both phases are very close. As discussed earlier in this section, the two signals from aqueous and vesicle phases at the high-field line significantly overlap (Fig. 4). Even though the applied magnetic field was set on each different peak, the recovery signal of

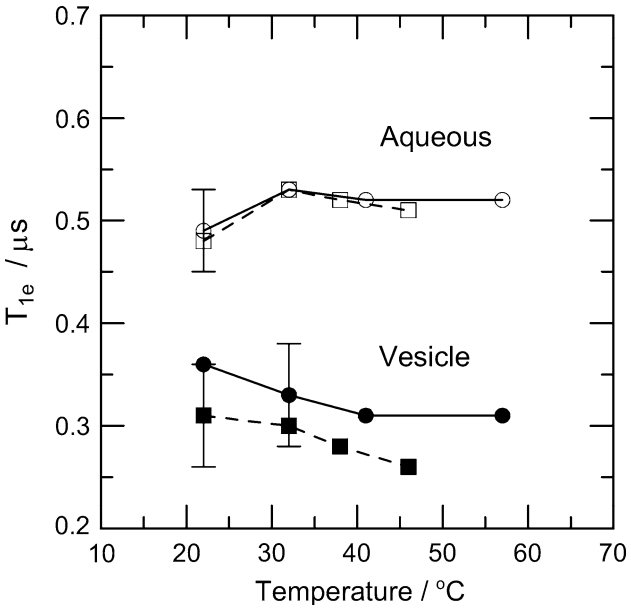

Fig. 11 Plot of T_{1e} for DTBN in H_2O (*circles*) and D_2O (*squares*) dispersions as a function of the temperature. The *open circles* and *open squares* represent T_{1e}'s in the aqueous phase. The *filled circles* and *filled squares* represent T_{1e}'s in the vesicle phase

may not be reliable for each phase. However, based on the correlation times, the relaxation time of TEMPO in the vesicle phase could show a longer value than that for DTBN.

Furthermore, the simultaneous observation of the two different signals along with the linewidth change at various temperatures is a perplexing problem for conventional EPR. In order to obtain further information about membrane dynamics, analyses of the overlap signals from the two different environments (the aqueous and vesicle phases) were attempted using 9-GHz EPR and SR spectroscopies. Despite the problems, new physicochemical evidence was extracted by the combination of various approaches.

CW EPR of Large Spin Probes

Figure 12 shows representative EPR spectra of HCO/DSA in aqueous dispersions at two different temperatures. EPR spectra of 7-DSA show that the spin probe site is more immobilized than those for 12-DSA and 16-DSA. This suggests that the tumbling motion of the nitroxide moiety of the probe increases as the position moves down the inner HCO membrane. The EPR spectrum of 7-DSA at 50 °C still shows parallel and perpendicular hyperfine components. Similar EPR spectra were observed for 12-DSA at lower temperatures. The EPR spectrum of 12-DSA at 50°C becomes more mobile and the spectral pattern shows neither parallel nor perpendicular components clearly. EPR spectra of 16-DSA at the temperature range studied show

Fig. 12 Representative EPR spectra of various doxylstearic acids observed in aqueous dispersed HCO are shown at two different temperatures. Parallel ($2A_{\|}'$) and perpendicular ($2A_{\perp}'$) hyperfine components are indicated as an example

that the spin site becomes more flexible. Thus, CW EPR results suggest that the probe moiety of 7-DSA is more rigid and going further down the membrane chain flexibility increases.

Conventional hyperfine analysis gives limited information concerning the probe environment in the HCO membrane. Modern computational analyses of the EPR results provide new qualitative information regarding the membrane dynamics. Thus, one can analyze the membrane dynamics using various outputs after the spectral simulation.

The representative calculated spectra are presented along with experimental spectra in Fig. 13. Satisfactory agreement between calculated and experimental spectra was obtained. The computational analyses of EPR lineshapes yield rotational diffusion coefficients as described in the experimental section. Two rotational diffusion coefficients ($R_{\perp}$ and $R_{\|}$) describe reorientation of the nitroxide radical around the axis perpendicular and parallel to the mean symmetry axis of the probe. A plot of $R_{\perp}$ as a function of inverse absolute temperature is shown in Fig. 14. The $R_{\perp}$ values for 7-DSA change from 1.9×10^7 to 4.0×10^7 s^{-1}. The $R_{\perp}$ values for 12-DSA change from 2.6×10^7 to 6.3×10^7 s^{-1}. The $R_{\perp}$ values for 16-DSA vary from 8.6×10^7 to 3.7×10^8 s^{-1}. The temperature dependence of the $R_{\perp}$ component of 12-DSA is slightly

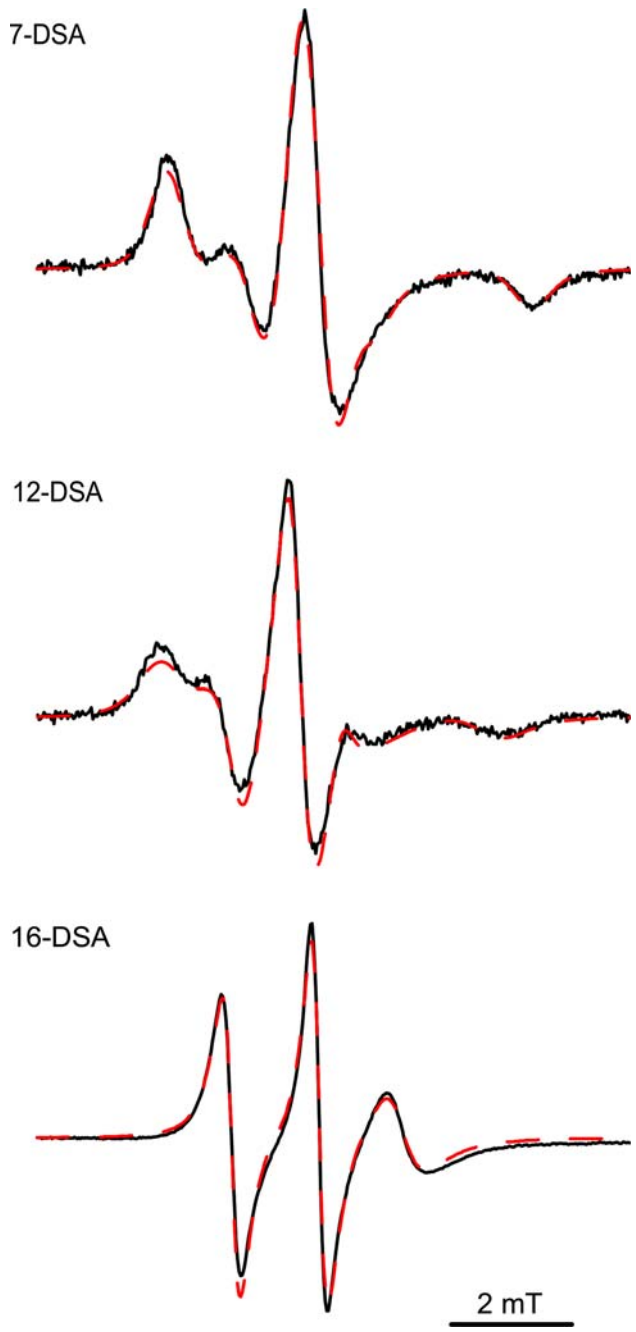

Fig. 13 Experimental (*solid line*) and simulated (*broken line*) EPR spectra of 7-DSA, 12-DSA, and 16-DSA in dispersions of HCO at 20 °C, respectively

stronger than that of 7-DSA. The $R_{\perp}$ of 16-DSA shows the strongest temperature dependence among spin probes studied.

Using rotational diffusion coefficients resulting from respective MOMD calculation, activation energies were obtained. Activation energies for the probes were calculated based on the slope of the plot (Fig. 14). An Arrhenius-type equation gives the activation energy (E_a) for the spin probe in the HCO membrane [12, 13]

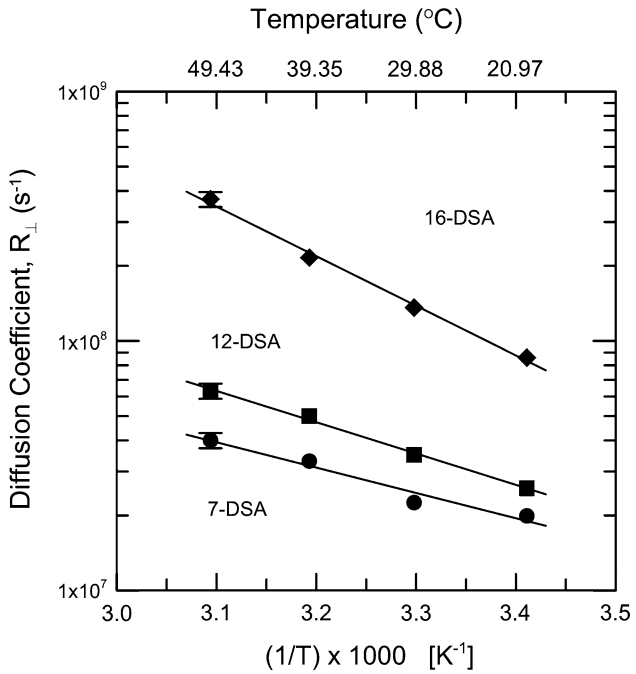

Fig. 14 Plot of rotational diffusion coefficient ($R_{\perp}$) versus inverse of absolute temperature obtained from the simulation. *Filled circles*, *filled squares* and *filled diamonds* represent 7-DSA, 12-DSA, and 16-DSA, respectively. The experimental errors are indicated

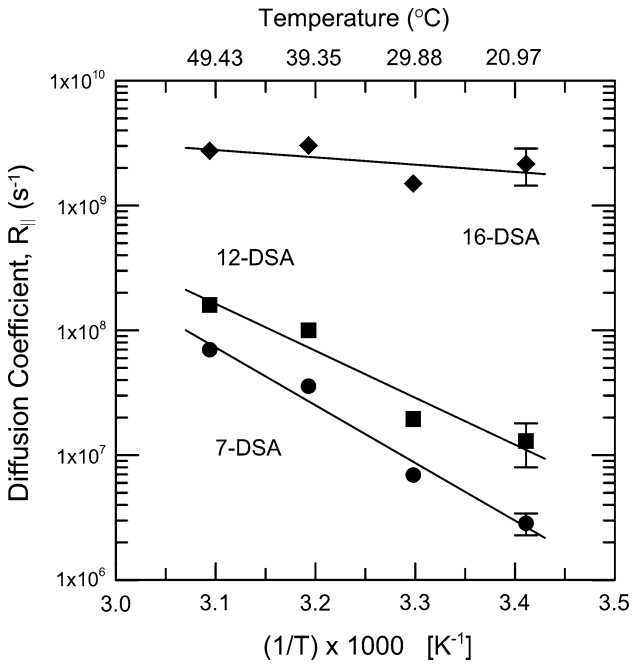

Fig. 15 Plot of rotational diffusion coefficient ($R_{\|}$) versus inverse of absolute temperature. *Filled circles*, *filled squares* and *filled diamonds* represent 7-DSA, 12-DSA, and 16-DSA, respectively

$$R_{\perp,\mathrm{II}} = R^{0}_{\perp,\mathrm{II}} \exp\left(\frac{-E_a}{RT}\right), \tag{9}$$

where E_a is the activation energy, R is the Gas constant, and T is the absolute temperature. The activation energies for 7-DSA, 12-DSA, and 16-DSA in the membrane are 19 ± 0.9, 24 ± 1.2, and 37 ± 1.8 kJ/mol, respectively. The higher activation energy calculated implies that the perpendicular motion of 16-DSA is more sensitive to temperature than that of other spin probes studied. The activation energies are associated with the micro-viscosity around the spin probes. The temperature dependence of the spin probes in the membrane implies that the immediate membrane environments for 12-DSA and 16-DSA are different. It is noted that the activation energy for the probe moiety of 16-DSA is higher than the activation energy (15–27 kJ/mol) estimated for C–C band rotation of alkyl chains [32]. This suggests that the parallel motion of the probe is subject to additional dynamic contribution from the membrane chain.

Figure 15 shows $R_{\|}$ components obtained by the EPR spectral simulation. The repeated computations show that the errors of parallel component values are larger than those for perpendicular components. The temperature dependence of 7-DSA and 12-DSA is 3–4 times stronger than that of the $R_{\perp}$ components. It is interesting to note that the $R_{\|}$ values for 16-DSA exhibit small temperature dependence. The results suggest that the parallel behaviors of the probe moieties for 7- and 12-DSA are sensitive to temperature and those for 16-DSA are less sensitive.

T_{1e} of Large Spin Probes

Direct observations of interaction between spin probe and lattice (membrane) were made. The spin-lattice relaxation times (T_{1e}) are sensitive to overall molecular tumbling of the probe and to internal motion within the membrane. The typical saturation recovery signals of 7-DSA and 16-DSA for the HCO membrane are shown in Fig. 16. The recovery signal was obtained at the magnetic field that corresponds to the centerline. The T_{1e} values were calculated using a single exponential fit for the SR signal. Signal-to-noise ratio of the SR signal for 7-DSA is poorer than that for 16-DSA because of weaker EPR intensity. The recovery time (~ 9 μs) for 7-DSA was much longer than that for 16-DSA at the same temperature. The longer T_{1e} for 7-DSA is consistent with the $R_{\perp}$ obtained. The longer T_{1e} values suggest the good organization and rigidity around the probe.

Figure 17 shows the plot of T_{1e} as a function of temperature. The results obtained are quite important in two respects. First, a significant difference of T_{1e} between 7-DSA and 12-DSA was observed. The T_{1e} gets about 4 μs shorter from 7-DSA to 12-DSA. This suggests that the middle region of the membrane chain is fairly fluid. The

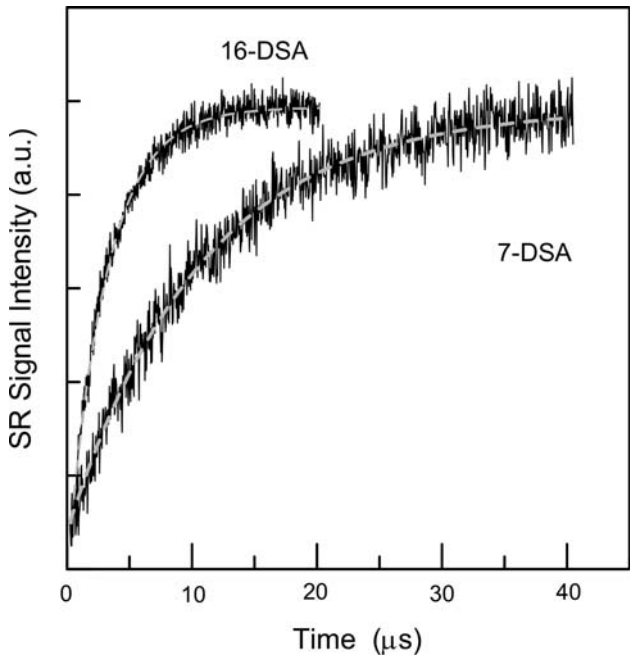

Fig. 16 Typical saturation recovery signals of 7-DSA and 16-DSA observed at 22 °C. The *broken line* indicates a single exponential fit to calculate the electron spin-lattice relaxation times (T_{1e}). The T_{1e} values are 3.6 and 9.1 μs for 16-DSA and 7-DSA, respectively

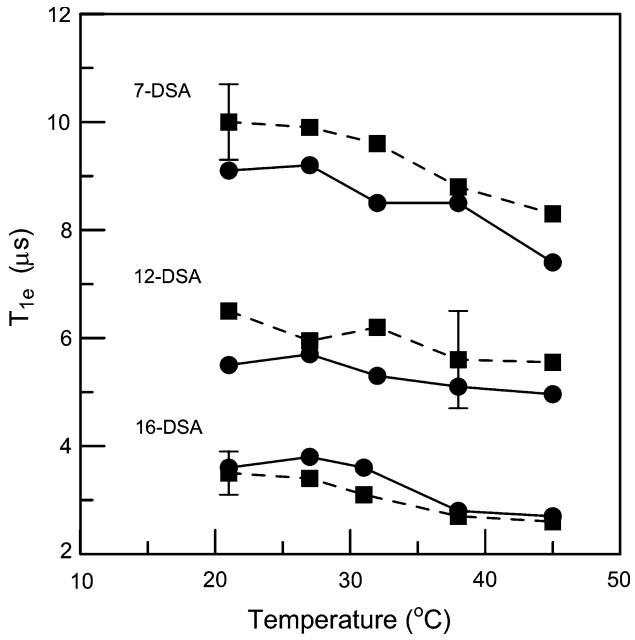

Fig. 17 Plot of spin-lattice relaxation times for various spin probes as a function of temperature. *Filled circles* and *filled squares* represent H_2O and D_2O, respectively. The experimental errors are indicated

T_{1e} gets shorter as the spin site goes toward the inner chain at the same temperature. It is notable that T_{1e} gets about 2 μs shorter from 12-DSA to 16-DSA. The motion of 12-DSA might be influenced by the terminal chain motion. Second, the relaxation results are different from the order parameter (S) obtained by hyperfine analyses [16]. However, the shorter T_{1e} for 16-DSA is consistent with the $R_\perp$ values. Thus, the relatively short T_{1e} suggest a fair degree of mobility in this probe region.

The T_{1e} also becomes shorter with increasing temperature. This is expected if increased motion of the probe occurs throughout the membrane environment. The values for 7-DSA and 16-DSA show clear temperature dependence. In addition, when T_{1e} becomes shorter with increasing temperature, the tumbling correlation time becomes shorter. Generally, the minimum T_{1e} value occurs at $\tau_c\omega_0 \approx 1$ where τ_c is the correlation time and ω_0 is the EPR resonance frequency [33].

Furthermore, T_{1e} was measured for D_2O dispersed HCO solution in order to examine the isotope effect. The T_{1e} obtained for H_2O and D_2O did not show clear a difference within experimental uncertainty as indicated in Figure 17. Thus, no position or temperature of the probes showed a significant T_{1e} difference.

HCO Dynamics of the Head Group Region

Detailed knowledge of the head group region is important for understanding the membrane functions and properties. In order to reveal the motional behaviors in the head group region, 5-DSA and CHL were used as the probes. Figure 18a shows the typical EPR spectrum of HCO/5-DSA in an aqueous dispersion at 20 °C. The EPR spectrum shows that the nitroxide probe is immobilized in the membrane and the parallel ($2A_{\|}$) and perpendicular ($2A_\perp$) hyperfine components as presented in the figure are clearly recognized. The EPR spectral pattern is slightly different from the rigid spectral pattern which was published previously [13, 16]. The pattern of the perpendicular hyperfine component which was obtained is clear. This indicates that the head group region is relatively flexible. It could be that the amphiphilic property is due to hydration in the head group region. Figure 18a also shows the EPR slow-tumbling simulation of the observed spectrum. The perpendicular rotational diffusion coefficient ($R_\perp$) obtained at 20 °C was 3.4×10^7 s^{-1}. The value of the chain ordering (S_0) was approximately 0.3–0.4 which suggests comparatively low rigidity of the region in the membrane.

Figure 18b shows the typical EPR spectrum of HCO/CHL in an aqueous dispersion at 20 °C. The spectral pattern obtained for CHL is similar to that previously reported [24]. The spectral pattern is different from the one for 5-DSA because the axes of CHL are not the same along the membrane z-axis as shown in Fig. 3. The EPR spectrum shows that the nitroxide is also immobilized in the membrane [13].The EPR spectral pattern also suggests that the

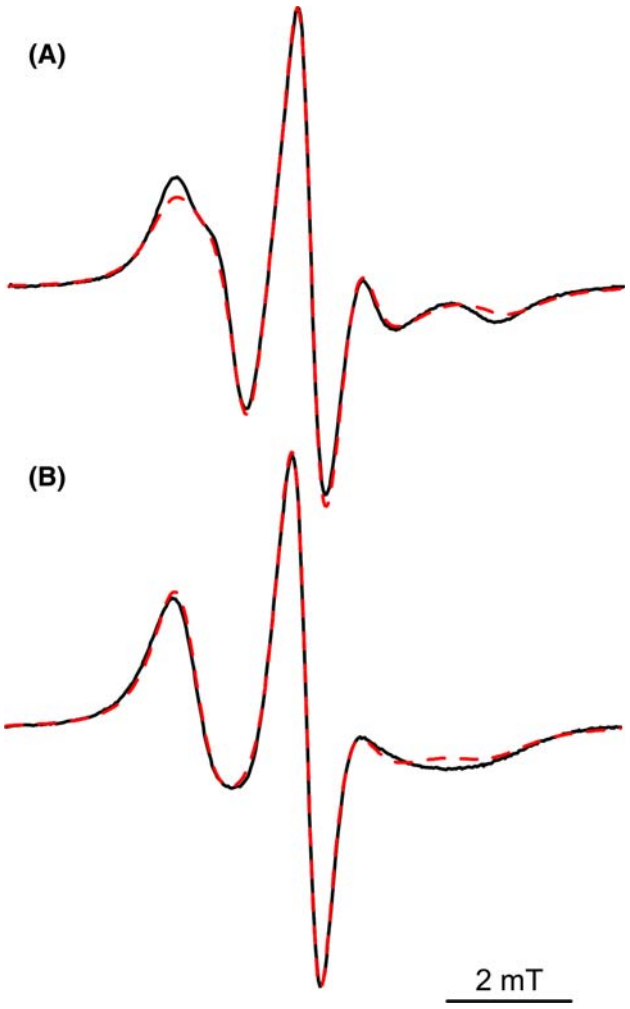

Fig. 18 Experimental (*solid line*) and simulated (*dotted line*) EPR spectra of **a** 5-DSA and **b** CHL in aqueous dispersions of HCO at 20°C are presented

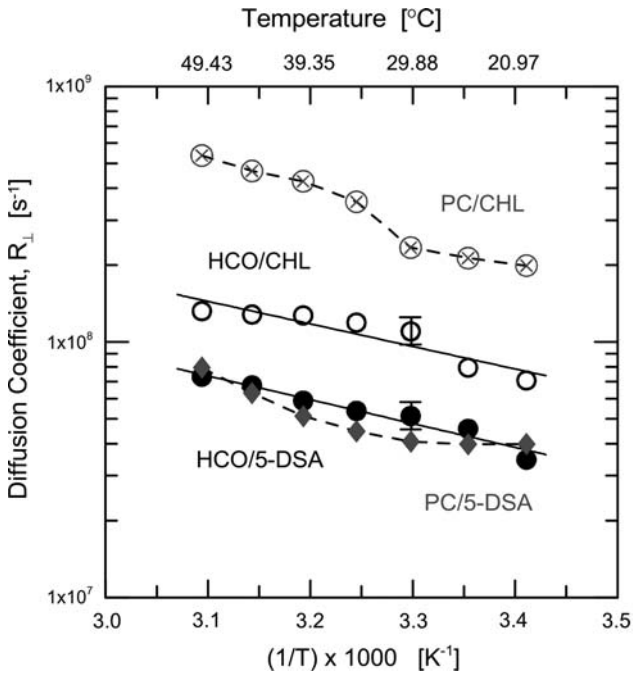

Fig. 19 Plot of the rotational diffusion coefficients ($R_\perp$), 5-DSA (*filled circles*) and CHL (*open circles*), in aqueous dispersions of HCO as a function of the inverse of the absolute temperature. The 5-DSA (*diamonds*) and CHL (*circles with cross symbol*) indicate the $R_\perp$ values for PC from egg

head group region is relatively flexible. This is consistent with the low S_0-value ($\sim$0.4) obtained. The flexibility can be due to hydration induced by the oxyethylene groups in the region. Figure 18b shows the EPR slow-tumbling simulation of the observed spectrum. The perpendicular rotational diffusion coefficient obtained at 20 °C was 7.0×10^7 s^{-1}.

Figure 19 presents perpendicular components of the diffusion coefficients for 5-DSA and CHL as a function of the temperature examined. The values of $R_\perp$ for CHL have slightly faster diffusion coefficients than the one for 5-DSA. These results can be associated with the probe orientation as well as the moiety in the membrane (Fig. 3). The diffusion coefficients for both probes show similar temperature dependence.

The activation energies using the diffusion coefficients resulting from the respective MOMD calculation were calculated based on the slope of the plot (Fig. 19). An Arrhenius-type equation gives the activation energy (E_a) for the spin probe in the HCO membrane [12]. The activation energies for 5-DSA and CHL in the membrane are 18 $\pm$ 0.5 and 17 $\pm$ 0.4 kJ/mol, respectively. The higher activation energy calculated implies that the perpendicular motion of 5-DSA has a similar value to 19 kJ/mol of 7-DSA [12]. The activation energies are associated with the micro-viscosity around the spin probes.

Egg PC Dynamics of Head Group Region

In order to reveal the motional behaviors in the head group region, 5-DSA and CHL were used as the probes. Both probes show similar EPR spectra of HCO aqueous dispersions. The EPR spectrum shows that the nitroxide probe is immobilized in the membrane and the parallel ($2A_{\|}$) and perpendicular ($2A_\perp$) hyperfine components as presented in the figure can be clearly recognized. The anisotropic EPR spectral pattern is slightly different from the rigid spectral pattern which was published previously [12]. The perpendicular hyperfine component was clearly observed. This indicates that the head group region is relatively flexible. The amphiphilic property may be due to hydration in the head group region. The EPR slow-tumbling simulation showed that the perpendicular rotational diffusion

coefficient ($R_\perp$) obtained at 20 °C was 3.4×10^7 s^{-1}. The value of the chain ordering (S_0) was approximately 0.3–0.4 which suggests comparatively low rigidity of the region in the membrane.

The values of $R_\perp$ for 5-DSA probe are similar for both HCO and PC in the temperature range examined (Fig. 19). It is interesting to note that the $R_\perp$ value for PC from egg starts to increase slightly at around 30 °C. The results imply that the motion of the probe changes as the temperature increases.

The $R_\perp$ value for HCO/CHL obtained at 50 °C was 1.3×10^8 s^{-1}. The $R_\perp$ value of 3.6×10^7 s^{-1} for DPPC/CSL obtained at 50 °C is reported [34]. The value for HCO/CHL suggests a slightly faster the motion. It is interesting to note that the values of $R_\perp$ for PC/CHL are much higher than those of HCO/CHL and show that the rate of the probe motion is faster than that of HCO. The values for PC/CHL increase significantly at approximately 30 °C (Fig. 19). The results obtained are consistent with those for HCO/5-DSA. The change can be correlated with a phase transition.

In addition, these results can be associated with the amphiphilic membrane properties. Most likely H_2O easily reaches the inner head group region. Because of the oxyethylene group in the region, significant dehydration may not occur even at higher temperatures. The surface region of the membrane can always make contact with H_2O. The rest of the lipids will change to a hydrophobic environment as the temperature rises. Therefore, the present EPR shows that the fluidity of the head group region does not change considerably throughout the temperatures examined.

T_{1e} of the Head Group Region

Next, direct observations of interactions between the spin probe and the lattice (membrane) were made by SR spectroscopy [16, 35, 36]. The spin-lattice relaxation times (T_{1e}) are sensitive to overall molecular tumbling of the probe at the specific position and to internal motion within the membrane. The recovery signal was obtained at the magnetic field that corresponds to the centerline. The typical SR signal of 5-DSA obtained at 20 °C is presented in Fig. 20. The T_{1e} values were calculated using a single exponential fit for the SR signal using Eq. 7. The T_{1e} values obtained are listed in Table 1 together with the various values obtained by EPR slow-tumbling simulation [12, 13, 18]. The T_{1e} for CHL is slightly longer than one for 5-DSA.

Figure 21 shows electron spin-lattice relaxation times (T_{1e}) of 5-DSA and CHL as a function of the temperature examined. The values of 5-DSA and CHL at 20 °C are 4.5 and 5.0 μs, respectively. Both probes have relatively short relaxation times and showed no abrupt change in the temperature range. This suggests that spin probes are

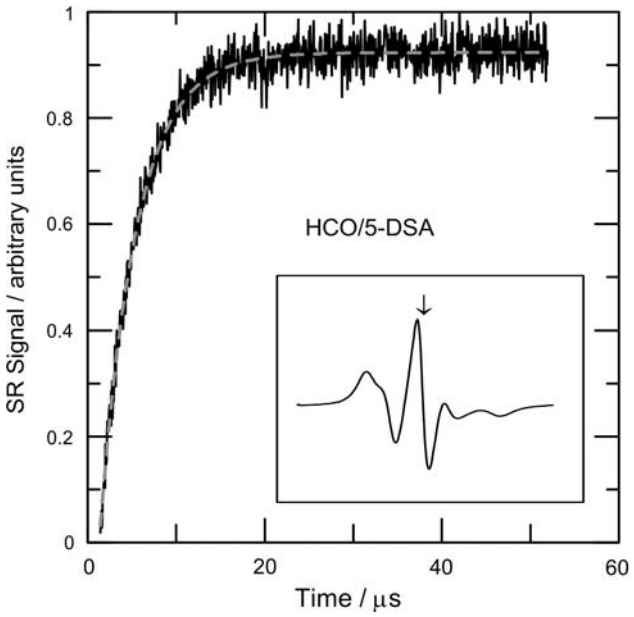

Fig. 20 Typical SR signal of 5-DSA observed at 20 °C. The *dashed line* indicates a single exponential fit to calculate the spin-lattice relaxation time (T_{1e}). The T_{1e} value is ~4.6 μs

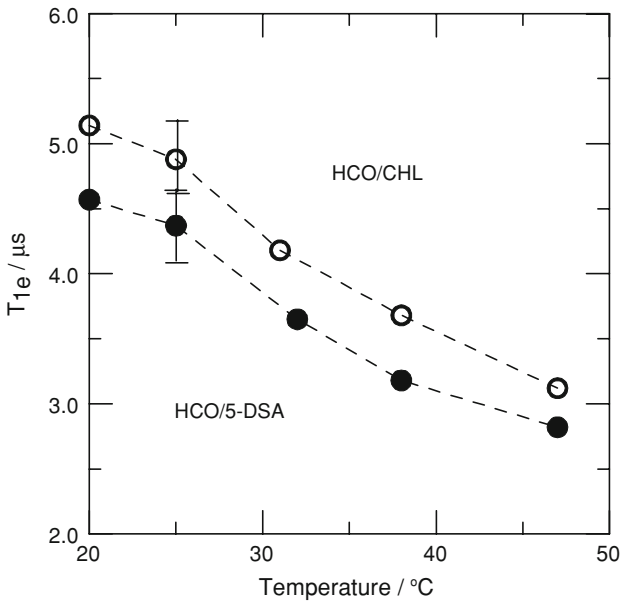

Fig. 21 Plot of the spin-lattice relaxation times (T_{1e}) of 5-DSA (*filled circles*) and CHL (*open circles*), in H_2O dispersions of HCO as a function of the temperature. The experimental errors are also indicated

mobile in the membrane. The probe behavior increases as the temperature increases. The temperature dependence of T_{1e} is moderate, suggesting the probe motions change moderately in the temperature range. The values (~5 μs) of T_{1e} for both probes were shorter than those for 7- and 12-DSA at the same temperature. The shorter T_{1e} values

are consistent with the faster diffusion rates obtained. Thus, the T_{1e} and rotational diffusion values suggest that the organization around the probe in the region is relatively flexible. The temperature dependence of T_{1e} for both probes is similar at the temperature examined. The values of T_{1e} for CHL at 20 °C became shorter when the temperature rises. This is expected if frequent interaction of the probe occurs when the membrane environment becomes fluid. The values for both probes show clear temperature dependence.

In addition, when T_{1e} becomes shorter with increasing temperature, the tumbling correlation time becomes shorter. These results can be associated with the amphiphilic membrane properties. Most likely H_2O easily accesses to the head group region. Taking account of the values for the same series of DSA probes, 5-DSA can be located in or nearer the head group region than that of 7-DSA. Based on the results, the possible 5-DSA location in the HCO membrane is illustrated in Fig. 22. Because of the oxyethylene group in the head group region, significant dehydration may not occur at higher temperatures. The surface region of the membrane can always make contact with H_2O. The rest of the lipids will change to a hydrophobic environment as the temperature rises. The results also suggest that overall water in the group may not change significantly as the temperature rises. Therefore, the present EPR and SR show that the head group fluidity does not change much as a function of temperature.

On the other hand, the T_{1e} value of CHL is slightly longer than that of 5-DSA. The relaxation time implies that the correlation time must be longer than that of 5-DSA. However, the diffusion coefficient obtained by the simulation was not slow. The results can be due to different molecular motions of CHL having aromatic rings and its location in the membrane. It was also suggested that EPR and EPR simulation for the cholesterol derived probe remain preferentially in the liquid ordered region of the detergent-resistant membrane [18]. The experimental errors are presented in Fig. 21. It is noted that the low sample concentration ($\sim$80 μmol dm^{-3}) of the probe provided a weak signal and was related to the errors.

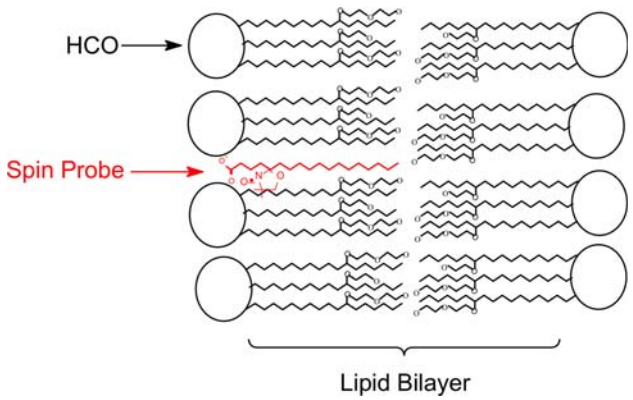

Fig. 22 Schematic illustration of 5-DSA incorporated in the HCO membrane

In previous research of HCO, the temperature dependence of rotational diffusion coefficient for 5-DSA and CHL showed a moderate decrease as a function of temperature [15]. In order to verify the results concerning the probes in the membrane, the probe behavior in egg PC, as a well-defined membrane, were examined. Both probes which incorporated PC from egg in aqueous dispersion were carried out in the same manner as the HCO membrane. The T_{1e} values obtained for PC/5-DSA and PC/CHL were approximately 2.3 μs at 20 °C. The T_{1e} of egg PC had a shorter relaxation time than those for HCO dispersion. It is also notable that the short relaxation time of $\sim$2.3 μs is close to the SR instrumental dead time [19]. The reliable relaxation time cannot be observed due to the short relaxation time. Thus, it is not possible to compare the relaxation behavior as a function of temperature with the egg PC which has phase transition at $\sim$37 °C.

Conclusions

The present EPR and saturation recovery results provide further detail on the characteristics and dynamic properties of the HCO membrane such as the partitioning, rotational correlation, rotational diffusion and segmental motions that varies along the membrane chain, and relaxation time of probes in the amphiphilic membrane. The conventional analyses measuring hyperfine couplings ($2A_{\|}$ and $2A_{\perp}$) provide limited information concerning the probe moiety in the membrane. Modern computational analyses of the EPR results provide new and qualitative information regarding membrane dynamics.

The electron spin-lattice relaxation times become shorter when the position of the probe moves toward the inner membrane as well as when the temperature increases. The spin dynamics were consistent with the EPR lineshape observed. The T_{1e} values for the probes were supported by the computational analyses such as diffusion coefficients and activation energy. No significant difference of T_{1e} between H_2O and D_2O was observed. The obtained T_{1e} values suggest that the interaction between the probe and H_2O (or D_2O) does not contribute to the major relaxation process in the membrane. The results of the order parameter and rotational diffusion coefficients were consistent with T_{1e} values obtained for both probes. Therefore, the EPR results provide insights into solving the long standing problem regarding quantitative understanding of the regional probe dynamics as well as the amphiphilic membrane characteristics. Finally, CW EPR, the modern slow-motional

simulation, and advanced EPR characterization of the HCO bilayer system provide qualitative intrinsic behaviors of the various spin probes in the membrane.

Acknowledgments The latest version of the NLLS program for the slow tumbling simulation was provided by Cornell University. The author would like to thank Dr. Mingtao Ge of Cornell University for helpful discussions concerning the results.

References

1. Weil JA, Bolton JR, Wertz JE(1986) Electron spin resonance. Chapman and Hall, New York
2. Dragutan I, Bokria JG, Varghese B, Szajdzinska-Pietek E, Schlick S (2003) Self-assembling in nafion perfluorinated ionomers based on ESR spectra of novel fluorinated nitroxide spin probes. J Phys Chem B 107:11397–11403
3. Varghese B, Schlick S (2002) Microphase separation in poly(acrylonitrile-butadiene-styrene) (ABS) studied with paramagnetic spin probes. II. Simulation of electron spin resonance spectra. J Polym Sci B 40:424–433
4. Hinderberger D, Spiess HW, Jeschke G (2004) Dynamics, site binding, and distribution of counterions in polyelectrolyte solutions studied by electron paramagnetic resonance spectroscopy. J Phys Chem B 108:3698–3704
5. Hinderberger D, Spiess HW, Jeschke G (2004) Separation of polyelectrolyte chain dynamics of counterion attachment by EPR spectroscopy. Macromol Symp 211:71–86
6. Crosas E, Egea MA, Reig F (2006) Spectroscopic techniques applied to the study of laminin fragments inserted into model membranes. J Colloid Interface Sci 295:264–269
7. Budil DE, Lee S, Saxena S, Freed JH (1996) Non-linear least squares of slow-motion EPR spectra in one and two dimensions using a modified Levenberg-Marquardt algorithm. J Magn Reson A 120:155–189
8. Shimshick EJ, McConnell HM (1973) Lateral phase separation in phospholipid membranes. Biochemistry 12:2351–2360
9. Subczynski WK (1992) Effects of polar carotenoids on dimyristoylphosphatidylcholine membranes: a spin-label study. Biochim Biophys Acta 1105:97–108
10. Barnes JP, Freed JH (1998) Dynamics and ordering in mixed model membranes of dimyristoylphosphatidylcholine and dimyristoylphosphatidylserine: a 250-GHz electron spin resonance study using Cholestane. Biophys J 75:2532–2546
11. Ligeza A, Tikhonov AN, Hyde JS, Subczynski WK (1998) Oxygen permeability of thylakoid membranes: electron paramagnetic resonance spin labeling study. Biochim Biophys Acta 1365:453–463
12. Nakagawa K (2003) Diffusion coefficient and relaxation time of aliphatic spin probes in a unique triglyceride membrane. Langmuir 19:5078–5082
13. Nakagawa K (2004) ESR spin probe investigation of chain ordering of triglycerol membrane. Bull Chem Soc Jpn 77:269–273
14. Freed JH (1976) The theory of slow tumbling ESR spectra for nitroxides. In: Berliner LJ (ed) Spin labeling, theory and applications, Chap 3. Academic Press, New York, pp 53–132
15. Tanaka M, Fukuda H, Horiuchi T (1990) Properties of the aqueous vesicle dispersion formed with poly(oxythylene)hydrogenated caster oil. J Am Oil Chem Soc 67:55–60
16. Nakagawa K (2002) Spin-lattice relaxation times of aliphatic spin probes in a unique triglyceride membrane. Chem Let 666–667
17. New RRC (ed) (1990) In: "Liposomes: a practical approach, Chap 2. Oxford University Press, Oxford, pp 33–104
18. Nakagawa K (2007) Spin-Probe Investigation of a Head Group Behavior in Aqueous Dispersion of a Nonionic Amphiphilic Compound. Lipids 42:457–462
19. Nakagawa K (2004) Partitioning, rotational correlation, and spin-lattice relaxation of small spin probes in dispersions of a triglyceride membrane. Bull Chem Soc Jpn 77:1323–1329
20. L. J. Berliner (1976) (ed) In: "Spin labeling, theory and applications, appendix II". Academic Press, New York, p 565
21. Nakagawa K (2005) Electron spin resonance investigation of small spin probes in aqueous and vesicle phases of mixed membrane made from poly(oxyethylene) hydrogenated castor oil and hexadecane. Lipids 40:745–750
22. Budil DE, Lee S, Saxena S, Freed JH (1996) Non-linear least squares of slow-motion EPR spectra in one and two dimensions using a modified Levenberg-Marquardt algorithm. J Magn Reson A 120:155–189
23. Meirovitch E, Igner D, Moro G, Freed JH (1982) Electron-spin relaxation and ordering in smectic and supercooled nematic liquid crystals. J Chem Phys 77:3915–3938
24. Meirovitch E, Freed JH (1984) Analysis of slow-motional electron spin resonance spectra in smectic phases in terms of molecular configuration, intermolecular interactions, and dynamics. J Phys Chem 88:4995–5004
25. Ge M, Freed JH (1998) Polarity profiles in oriented and dispersed phosphatidylcholine bilayers are different. An ESR study. Biophys J 74:910–917
26. Ge M, Rananavare SB, Freed JH (1990) ESR studies of stearic acid binding to bovine serum albumin. Biochim Biophys Acta 1036:228–236
27. Quine RW, Eaton SS, Eaton GR (1992) Saturation recovery electron paramagnetic resonance spectrometer. Rev Sci Instrum 63:4251–4262
28. Rinard GA, Quine RW, Eaton SS, Eaton GR, Froncisz W (1994) Relative benefits of overcoupled resonators vs inherently low-Q resonators for pulsed magnetic resonance. J Magn Reson A 108:71–81
29. Tanaka M, Fukuda H, Horiuchi T (1990) Properties of the aqueous vesicle dispersion formed with poly(oxythylene)hydrogenated caster oil. J Am Oil Chem Soc 67:55–60
30. Nakagawa K (2002) EPR and saturation recovery investigations of spin probes in dispersions of hydrogenated castor oil. In: Kawamori A, Yamauchi J, Ohta H (eds) EPR in the 21st century: basic and applications to material, life and earth sciences. Elsevier, Amsterdam, pp 494–499
31. Dix JA, Kivelson D, Diamond JM (1978) Molecular motion of small nonelectrolyte molecules in lecithin bilayers. J Membr Biol 40:315–342
32. Pace RJ, Chan SI (1982) Molecular motions in lipid bilayers. III. Lateral and transverse diffusion in bilayers. J Chem Phys 76:4241–4247
33. Slichter PC (1990) Principles of magnetic resonance, 3rd edn, Chap 5. Springer, Berlin Heidelberg New York, pp 137–187
34. Costa-Filho AJ, Shimoyama Y, Freed JH (2003) A 2D-ELDOR study of liquid ordered phase in multilamellar vesicle membrane. Biophys J 84:2619–2633
35. Robinson BH, Haas DA, Mailer C (1994) Molecular dynamics in lipids: spin-lattice relaxation of nitroxide spin labels. Science 263:490–493
36. Eaton GR, Eaton SS (2000) Relaxation times of organic radicals and transition metal ions. In: Eaton GR, Eaton SS, Berliner LJ (eds) Distance measurements in biological systems by EPR. vol 19, Chap 2. Plenum Press, New York, pp 29–154